Superconductivity in Li_8H_n electrides: The effect of interstitial anionic electrons on electron-phonon coupling

Zixuan Guo,[1] Aitor Bergara,[2,3,4] Xiaohua Zhang,[1,*] Xing Li,[1] Shicong Ding,[1] and Guochun Yang[1,5,†]

[1]*State Key Laboratory of Metastable Materials Science & Technology and Key Laboratory for Microstructural Material Physics of Hebei Province, School of Science, Yanshan University, Qinhuangdao 066004, China*

[2]*Physics Department and EHU Quantum Center, Universidad del País Vasco-Euskal Herriko Unibertsitatea, UPV/EHU, 48080 Bilbao, Spain*

[3]*Donostia International Physics Center (DIPC), 20018 Donostia, Spain*

[4]*Centro de Física de Materiales CFM, Centro Mixto CSIC-UPV/EHU, 20018 Donostia, Spain*

[5]*Centre for Advanced Optoelectronic Functional Materials Research and Key Laboratory for UV Light-Emitting Materials and Technology of Northeast Normal University, Changchun 130024, China*

(Received 23 January 2024; accepted 25 March 2024; published 4 April 2024)

The discovery of superconductivity in electrides, where partial electrons are localized in lattice interstices, labeled as interstitial anionic electrons (IAEs), introduces a different category known as electride superconductors. Understanding the role of IAEs in electron-phonon coupling (EPC) is crucial for the development of electride superconductors. In this study, we demonstrate that an increased net charge of IAEs enhances EPC in 12 Li_8H_n ($n = 4$–7) electrides, exhibiting cubic/tetragonal symmetry and diverse IAEs topologies. First-principles calculations reveal a nearly linear rise in the EPC constant with the net charge of IAEs. This increase stems from the excitation effect of IAEs on Li $2p$ electrons and their collaborative involvement in the formation of Cooper pairs, facilitated by Li-derived low/medium-frequency phonons. This mechanism is prominently illustrated in Pm-$3m$ Li_8H_4, featuring a T_c of 40.3 K, where Li atoms exhibit compressing and stretching vibrations, inducing IAEs dimerization and the strongest local EPC interaction. Conversely, hydrogen atoms in Li_8H_n electrides primarily regulate the net charge and topology of IAEs. Our findings bear significant implications for the advancement of electride superconductors.

DOI: 10.1103/PhysRevB.109.134505

I. INTRODUCTION

Superconductors, characterized by zero resistance and complete diamagnetism, play an indispensable role in commercial devices, and open avenues for innovative electronic applications [1–3]. The critical temperatures (T_cs) of these superconductors directly impact the operating costs and potential applications of devices. Consequently, the quest for high-temperature superconductors remains a perpetual focus in the realms of condensed matter physics and material science. However, the effective manipulation of electron-phonon coupling (EPC) holds paramount significance in facilitating the design of high-temperature superconductors [4,5]. The groundbreaking achievement in this pursuit has been the emergence of hydride superconductors. This achievement can be attributed to the incorporation of weak-covalence hydrogen cages, stabilized by carefully selecting electropositive elements. This strategic selection allows electrons to occupy antibonding orbitals of hydrogen molecules [6–10].

Electrides constitute a captivating category of compounds wherein a portion of their electrons resides in lattice interstices, acting as interstitial anionic electrons (IAEs) [11,12]. These IAEs exhibit diverse dimensional configurations (e.g., 0D [13], 1D [14], 2D [15], and 3D [16]), showcasing extraordinary attributes distinct from orbital electrons [17,18]. Moreover, they can hybridize with orbital electrons, introducing a unique dimension for property regulation [19]. The confirmation of the superconductivity attributed to IAEs not only expands the repertoire of superconducting materials but also contributes to a broader understanding of the EPC mechanism [20,21].

Since the discovery of superconductivity in electrides like $[Ca_{24}Al_{28}O_{64}]^{4+}(4e^-)$ [22], substantial research progress has been achieved in the realm of electride superconductors [23–25], particularly under high pressures [26–35]. Notably, certain electrides exhibit T_c values that surpass the McMillan limit, such as $P6/mmm$ Li_5C [36] and Li_5N [37], Li_8Cs [38], Li_8Ag [21], and various phases of Li_6P, $C2/c$ [39] and R-$3m$ [40]. Some electrides even approach or exceed the temperature of liquid nitrogen (e.g., Li_8Au [21]), hinting at their potential for high-temperature superconductivity. Simultaneously, a deeper understanding of the stability mechanism of electrides [41] and the origin of their superconductivity [33] has emerged. However, the role of IAEs in superconductivity remains contentious, with debates on whether IAEs enhance or impede superconductivity [23,42,43]. In light of this, establishing a clear relationship between IAEs and superconductivity becomes imperative for the realization of high-temperature electride superconductors.

Considering the factors mentioned above, we propose an approach to investigate the role of IAEs in the superconductivity of electrides. Our strategy involves utilizing the

*Corresponding author: zhangxh318@ysu.edu.cn
†Corresponding author: yanggc468@nenu.edu.cn

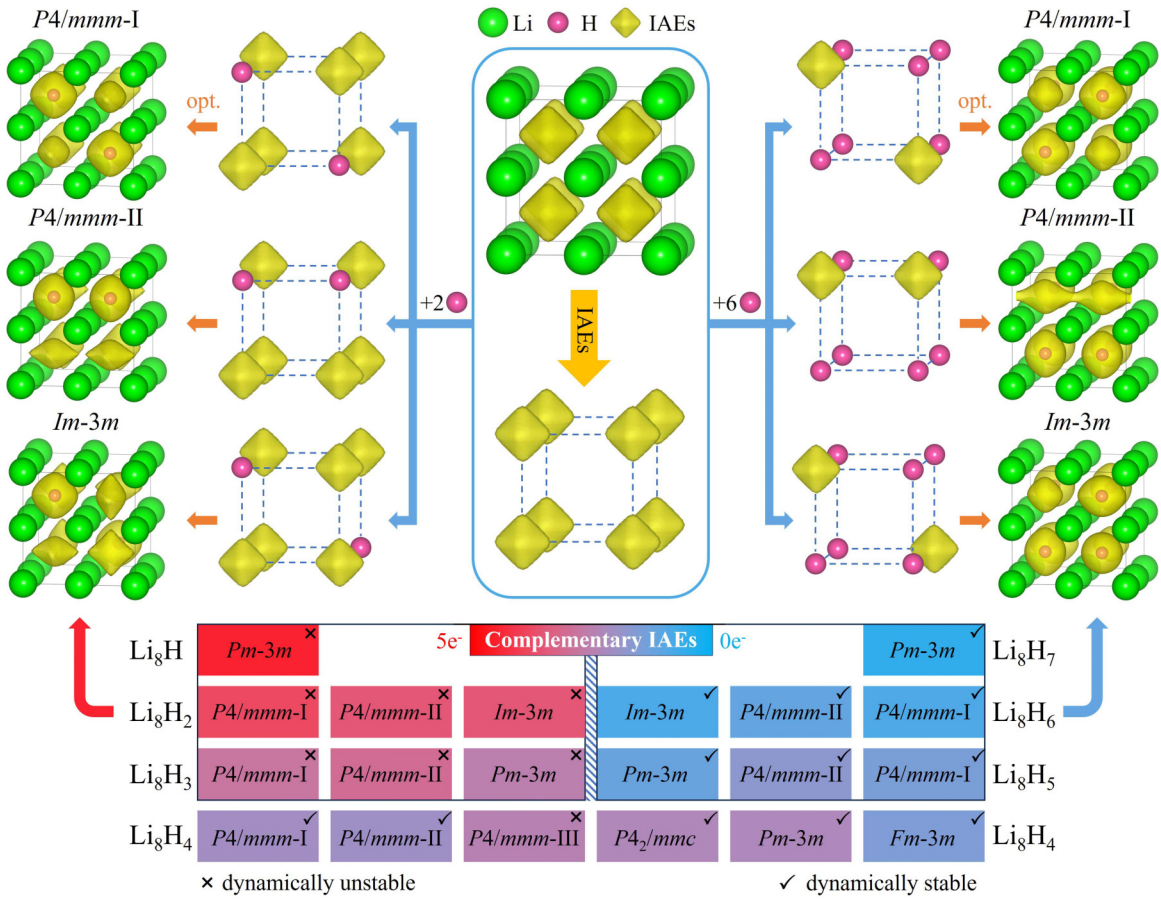

FIG. 1. The schematic diagram illustrates the design of Li_8H_n electrides, showcasing examples for $n = 2$ and 6. The parent *sc*-Li_8 is depicted with an ELF isosurface in the middle panel. The geometric relaxation is indicated by "opt." For clarity, the diagram summarizes the structural symmetry, IAEs charge (per Li_8H_n), and the dynamical stability of all optimized Li_8H_n electrides.

simplest elements, lithium and hydrogen, each with one valence electron, arranged in high-symmetry structures at the same pressure. We aim to modulate the hydrogen content to control the net charge of IAEs. Through first-principles calculations, we identify 12 Li_8H_n electrides characterized by distinct IAEs charge and topology, which can be modified by adjusting the hydrogen content. Surprisingly, our findings reveal a positive correlation between the EPC and the net charge of IAEs. Particularly noteworthy is the strong coupling observed in *Pm*-3*m* Li_8H_4, attributed to Li-derived low/medium-frequency phonons and the involvement of IAEs and Li 2*p* electrons. Their coupling results in a T_c of 40.3 K, surpassing the McMillan limit. Our research contributes to a deeper understanding of superconductivity associated to IAEs.

II. RESULTS AND DISCUSSION

We establish a family of Li_8H_n electrides based on a $2 \times 2 \times 2$ supercell of simple-cubic (*sc*) Li (*sc*-Li_8) serving as the host framework and hydrogen atoms as regulators for IAEs at a pressure of 300 GPa. The calculated electron localization function (ELF = 0.68, Fig. 1) confirms *sc*-Li_8 as an electride with eight IAE blocks positioned at the centers of small Li_8 cages. Each IAE block exhibits a regular octahedronlike topology, resembling the superposition of three *p*-orbital wave functions, and is hybridized with Li 2*p* orbitals (discussed later), imparting a *p*-orbital attribute. Bader charge analysis reveals that each IAE block carries a charge quantity of $0.67e^-$, functioning as a non-nuclear attractor with the capacity to attract electronegative atoms [44]. Recognizing the dynamic instability of pure *sc*-Li_8 electride [21], we introduce hydrogen atoms to accept partial IAEs, stabilizing the *sc*-Li_8 framework and allowing for the modulation of IAE distribution and charge. Hydrogen is chosen due to its minimal atomic radius and its contribution to a high Debye frequency, inducing high-temperature superconductivity [45,46]. Considering that enough hydrogen atoms can take up all IAEs provided by the metal framework, leading to the disappearance of the electride state [47], such as LaH_{10} [48] and Li_2MgH_{16} [49], the hydrogen content is controlled to not exceed Li_8H_7. For the stoichiometries Li_8H_n and Li_8H_{8-n} ($n = 1, 2, 3$), the occupation sites of H atoms and IAEs are interchanged, resulting in complementary IAE charge, as illustrated by Li_8H_2 and Li_8H_6 (Fig. 1). Additional details on the structure construction process (Fig. S1) and comprehensive computational information can be found in the Supplemental Material [50].

Following geometry relaxation, all designed Li_8H_n electrides maintain the orthorhombic Li framework. Hydrogen atoms exist in the form of anions, each acquiring a charge

of approximately $\sim 0.91e^-$, leading to an inverse relationship between the IAE charge and the hydrogen content (Fig. 1 and Fig. S2 of the Supplemental Material [50]). Among the 20 candidate structures, 12 exhibit dynamical stability, encompassing five high-symmetry cubic phases [i.e., *Pm*-3*m* Li_8H_n ($n = 4$, 5, 7), *Fm*-3*m* Li_8H_4, and *Im*-3*m* Li_8H_6], as well as seven low-symmetry tetragonal structures [i.e., *P*4/*mmm*-I and -II Li_8H_n ($n = 4$, 5, 6) and $P4_2/mmc$ Li_8H_4) (Figs. 1, S3, and S4). These dynamically stable structures also demonstrate high thermodynamic stability compared to LiH and elemental Li (Fig. S5), indicating their feasibility for experimental synthesis. It is noteworthy that the net charge of IAEs in Li_8H_n electrides significantly influences their dynamical stability. Specifically, the IAEs charge in the eight dynamically unstable structures (exceeding $2.45e^-$ per Li_8H_n, Fig. S2) is notably higher than that in the dynamically stable structures. This can be attributed to two facts: (1) IAEs have a weaker attraction with Li^+ ions compared to hydrogen anions due to their less negative charge (Table S1 [50]), and (2) hydrogen atoms occupy lower orbital levels than IAEs, favoring a decrease in the structural energy, as later elucidated by the projected density of states (PDOS) [Fig. 4(a)].

Remarkably, Li_8H_n electrides exhibit a diverse range of IAE topology and connectivity, stemming from the distinct structural symmetries induced by hydrogen atoms. In comparison to the regular octahedronlike IAEs in *sc*-Li_8, most Li_8H_n electrides showcase deformed octahedral topologies, such as elongated, squashed, and rounded configurations, influenced by the presence of hydrogen atoms and varying degrees of side lengths in the small Li_8 cages (Fig. S6). This diversity results in a plethora of IAE topologies, including 0D rounded and elongated octahedra in *Pm*-3*m* Li_8H_7 (Fig. S6b) and Li_8H_5 (Fig. S6d), and *P*4/*mmm*-I Li_8H_6 (Fig. S6g), 1D linear chains in *P*4/*mmm*-II Li_8H_6 (Fig. S6h), *P*4/*mmm*-I Li_8H_4 (Fig. S6l) and $P4_2/mmc$ Li_8H_4 (Fig. S6m), 2D square networks in *P*4/*mmm*-II Li_8H_5 (Fig. S6j), and the coexistence of 0D octahedra and 1D chains/2D networks in *P*4/*mmm*-I Li_8H_5 (Fig. S6i) and *P*4/*mmm*-II Li_8H_4 (Fig. S6k). Conversely, the five cubic phases exhibit more regular IAE topologies due to their higher structural symmetry. Overall, the IAEs in all Li_8H_n electrides possess a *p*-orbital attribute, resulting from the tension or compression deformation of octahedral IAEs within the small cubic Li_8 cage.

The calculated electronic band structures reveal that the 12 dynamically stable Li_8H_n electrides exhibit metallic behavior (Fig. S7), presenting a valuable opportunity to investigate IAEs-related EPC interaction—an essential factor determining T_c [58]. In the case of the five cubic phases, their EPC constants (λ) demonstrate a near-linear increase with IAE charge [Fig. 2(a)], exhibiting a fitted slope of 0.385 and a substantial linear correlation coefficient ($r^2 = 0.95$). This trend resembles the behavior observed in superconducting H_xTe_y compounds characterized by H-dominated EPC [59]. Similarly, for the six *P*4/*mmm* phases, a clear positive correlation between λ and IAEs charge is evident, albeit with a smaller slope of 0.191 and an r^2 of 0.87 [Fig. 2(b)]. Notably, our findings provide direct evidence supporting the idea that IAEs with a *p*-orbital attribute enhance EPC interaction in electrides. The disparity in slopes between cubic and *P*4/*mmm* phases suggests that high structural symmetry holds a more

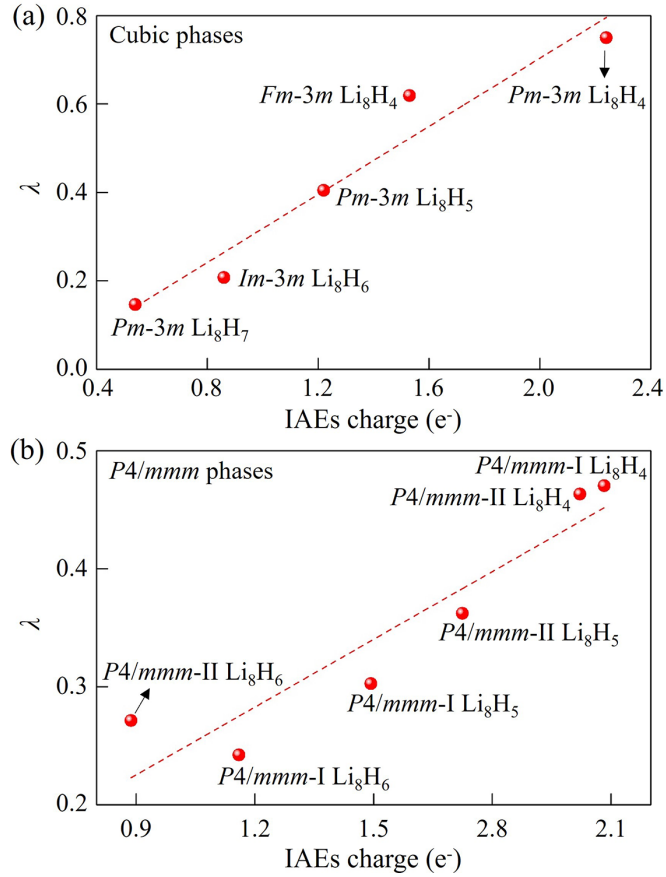

FIG. 2. The dependence of the EPC constant on IAEs charge in (a) five cubic structures and (b) six *P*4/*mmm* phases. The red dashed lines represent the fitted linear relations.

significant advantage, as demonstrated in superhydride superconductors [60]. This observation aligns with the fact that many high-T_c electrides possess high symmetry, as seen in *Fm*-3*m* Li_8Au and Li_8Ag [21], and *P*6/*mmm* Li_5C [36] and Li_5N [37].

Building upon the observed linear relationship between λ and IAE charge in the five cubic structures, our focus shifts to the investigation of their electride states, electronic structures, and superconductivity. Illustrated in Fig. 3, the four cubic phases from *Pm*-3*m* Li_8H_7 to *Fm*-3*m* Li_8H_4 exhibit individual and rounded-octahedron IAEs. However, there is a continuous and uniform increase of IAE sites within the cubic cell—progressing from the body center (1) to body center + vertex (2), face centers (3), and finally body center + edge centers (4). This leads to a quasilinear increase in IAE charge. In the case of Li_8H_4 transitioning from *Fm*-3*m* to *Pm*-3*m* (Fig. 3), the IAEs at edge centers shift to face centers. Simultaneously, the rounded-octahedron IAEs break down into two shapes: a regular octahedron (IAE1) and an elongated one (IAE2), accompanied by a faster augmentation of the IAEs charge. These outcomes indicate an effective regulation to the IAEs by the introduced H atom in *sc*-Li_8, achieved by controlling its content and occupation site.

Atom-resolved density of states at the Fermi level, $N(E_F)$, is calculated in these cubic Li_8H_n electrides to gain insight into the dependence of the EPC strength on the IAEs charge,

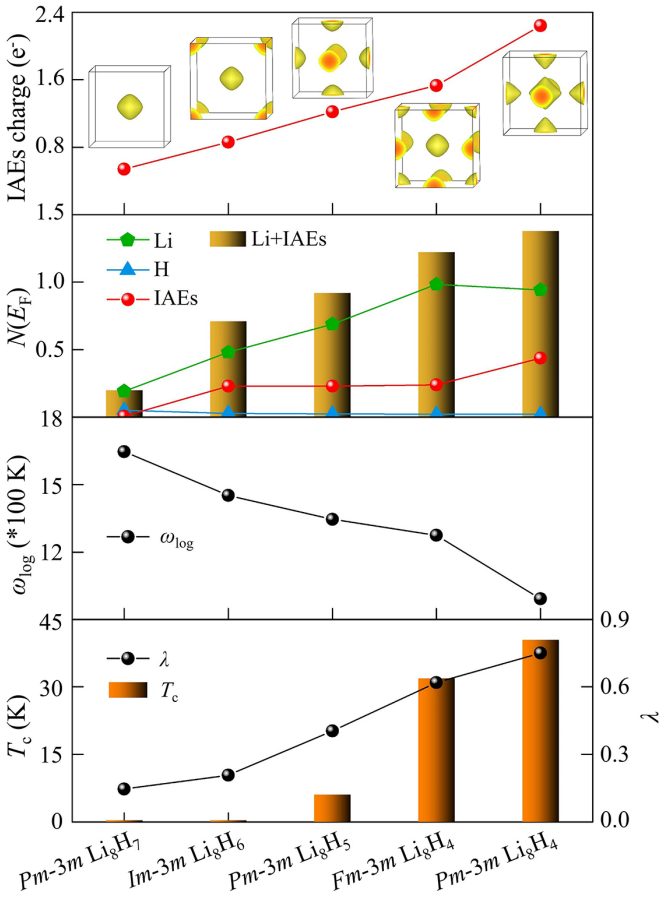

FIG. 3. The IAE charge and ELF isosurfaces (ELF = 0.68), atom-resolved $N(E_F)$ (unit: states/eV Li_8H_n), ω_{log}, EPC constant (λ), and T_cs of 5 cubic Li_8H_n electrides at 300 GPa. The Li and H atom are veiled to highlight the IAEs in ELF diagrams.

based on the formula $\lambda = \frac{N(E_F)\langle I^2\rangle}{M\langle\omega^2\rangle} = \eta N(E_F)$ [35]. Notably, IAE-derived $N(E_F)$ remains unchanged from Im-3m Li_8H_6 to Fm-3m Li_8H_4, in contrast to the monotonical increase in their IAEs charge (Fig. 3). Li atoms exhibit a decreased $N(E_F)$ from Fm-3m Li_8H_4 to Pm-3m Li_8H_4, while hydrogen atoms have a decreasing and negligible $N(E_F)$ due to their filled s orbital. Importantly, none of these factors alone can determine the change in λ. Considering that IAEs are coordinated by the surrounding eight Li atoms, and under the same Li content, Li-derived $N(E_F)$ exhibits an increasing trend with IAE charge (e.g., from Pm-3m Li_8H_7 to Fm-3m Li_8H_4). This suggests a potential excitation effect of IAEs on Li's electrons due to multiple interactions between IAEs and Li atoms, including coulombic interaction, orbital hybridization, and the coupling interaction of IAEs with vibrations of Li atoms (discussed later) [61]. Consequently, both IAEs and Li atoms should be considered as a whole. As expected, the sum of $N(E_F)$ for IAEs and Li atoms demonstrates a coincident change with λ, indicating that IAEs not only participate in the formation of Cooper pairs but also excite the participation of electrons in Li atoms. This mechanism is further supported by the increasing trend of λ and the $N(E_F)$ sum of IAEs and Li atoms in the six $P4/mmm$ phases, despite a few fluctuations (Fig. S8).

The mechanism through which IAEs enhance EPC can be further elucidated by drawing an analogy to the correlation proposed by Errea *et al.* between T_c and the electronic bonding network [62]. In this context, the T_c of superhydrides is determined by three key factors: hydrogen fraction, hydrogen-derived density of states at the Fermi level, and the electronic bonding network. Unlike traditional anions (e.g., F^-, H^-) characterized by strong electron localization, IAEs exhibit weaker localization and higher activity, as evidenced by their elevated energy levels [15]. This characteristic facilitates their hybridization with atomic valence orbitals [17,63]. Consequently, an increased net charge of IAEs, combined with a greater number of Li 2p electrons, forms a hybrid conductive network, thereby strengthening their coupling with the vibrations of surrounding Li atoms. Although $Li_{10}X$ (X = Te, Sb, and As) electrides consisting of different anionic atomic numbers also show the positive correlation between IAE charge and EPC [33], the effect of cations atomic number on this relation should be further explored due to their different pressure-dependent electron transition behaviors [64].

Subsequently, adopting the Allen-Dynes-McMillan formula with a typical Coulomb pseudopotential $\mu^* = 0.1$ [58,65], the T_c values of the Li_8H_n electrides are estimated (Fig. 3 and Table S2). Their T_c values are positively correlated with λ and IAE charge, but negatively associated with the logarithmic average phonon frequency (ω_{log}). Therefore, the superconductivity of these cubic Li_8H_n electrides can be manipulated by adjusting the IAE charge. The maximum T_c value is up to 40.3 K in Pm-3m Li_8H_4, which is comparable to the emblematic MgB_2 (39 K) [66], Li_6P electrides with $C2/c$ (39.3 K) [39], and R-3m symmetries (41.36 K) [40]. With lowering pressure, the T_c value of Pm-3m Li_8H_4 decreases monotonically to 10.7 K at 50 GPa (Fig. S9), which is originated from the weakening EPC. Furthermore, although the tetragonal $P4/mmm$ structures exhibit more diverse IAE topology, as mentioned above, they also show an increasing trend of T_c values with IAE charge, dominated by the increase of λ (Fig. S8). These results explicitly reveal a dependence of electride superconductivity on IAE charge under similar structural symmetry conditions.

Using Pm-3m Li_8H_4 as a representative with the maximum T_c, we delve into its electronic structures to unravel the mechanism of IAEs contributing to superconductivity. Three bands, labeled *i*, *ii*, and *iii,* cross the E_F [Fig. 4(a)], displaying flat features at R and M points and steep ones along $X \rightarrow R$ and $M \rightarrow \Gamma \rightarrow R$ directions. These bands are dominated by IAEs and Li 2p electrons, exhibiting an obvious hybridization [PDOS in Fig. 4(a)], supporting the p-orbital attribute of IAEs. In contrast, the filled 1s shell places the hydrogen atom far below the E_F. The presence of the icositetrahedronal electron pocket around the R point, formed by eight trigonal pyramid-like Fermi surface (FS) sheets in band *iii*, indicates that the electrons have a lower Fermi velocity [Figs. 4(b) and S10], which is favorable for strong EPC [67,68].

The calculated phonon dispersion curves and density of states (PHDOS) show a clear separation between Li-dominated low-/medium-frequency phonons (<40 THz) and H-dominated high-frequency phonons (>60 THz) [Figs. 4(c) and 4(d)]. The strong EPC is derived from Li-dominated vibrations [Fig. 4(c)], supported by the calculated Eliashberg

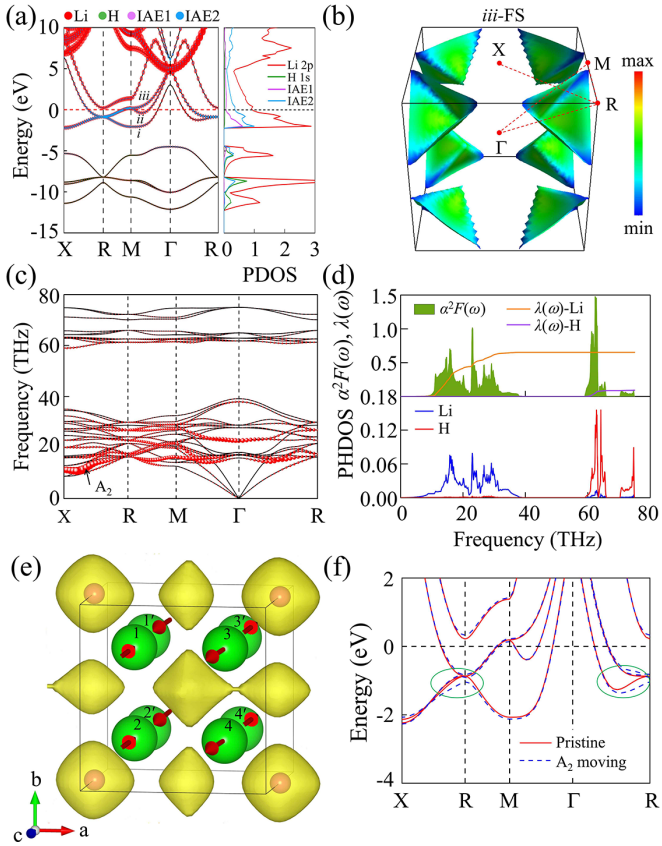

FIG. 4. (a) The projected electronic band structure and PDOS, (b) Fermi velocity-projected Fermi surface corresponding to the band *iii* in (a), (c) phonon dispersion curves with partial EPC, $\lambda_{q,v}$, proportional to the area of the circles, (d) PHDOS, Eliashberg spectral function $\alpha^2F(\omega)$, and frequency-dependent EPC, $\lambda(\omega)$, (e) ELF isosurface (ELF = 0.68) after a Li atom movement of about 0.05 Å along the A_2 mode (labeled with red arrows), and (f) the unfolding band structures with the atomic displacements along the A_2 mode, plotted along the same k path of the equilibrium structure to facilitate comparison.

spectral function $\alpha^2F(\omega)$, contributing up to 87.8% to total λ [Fig. 4(d)]. Despite having the maximum $\alpha^2F(\omega)$, H-dominated vibrations contribute only 12.2% to total λ due to their high frequency, according to the formula $\lambda = 2\int d\omega \frac{\alpha^2F(\omega)}{\omega}$ [58].

The formation of Cooper pairs is mediated by phonons, which are generated by lattice vibrations. Thus, the study of the vibrational mode has become an effective method to explore the superconducting origin [69–71]. Notably, the strongest partial EPC ($\lambda_{q,v}$), located at the softened acoustic branch between X and R points, is driven by the A_2 mode [Fig. 4(c)]. This mode corresponds to the compressing and stretching vibrations of Li atoms in pairs along the direction approximating the c axis [Fig. 4(e)]. The A_2 mode makes a dominant contribution to EPC, as the compressional vibrations of Li pairs (e.g., 1-1′, 2-2′) push IAE1 apart from IAE2 due to the increasing repulsion of nuclear electrons, while the stretching vibrations of 3-3′ and 4-4′ pairs induce IAE1 and IAE2 to form a dimer [Fig. 4(e)], facilitating electron exchange between vicinal IAEs regions. Additionally, the action of Li atoms on IAEs causes a distortion of IAE1 and IAE2 topology [Fig. 4(e)], enabling electron redistribution between Li atoms and IAEs (Fig. S11). This analysis is supported by the noticeable shifts in the flat bands at the R point, associated to IAEs and Li $2p$ electrons, when Li atoms experience a small displacement (∼0.05 Å) along the A_2 mode [marked in green circles, Fig. 4(h)]. This shift is indicative of a phonon strongly coupled to Fermi surface causing a significant energetic shift in k for the states near the E_F [72,73]. Consequently, the superconductivity of Pm-3m Li_8H_4 results from the coupling of the low-velocity electrons contributed by Li $2p$ orbitals and IAEs with phonons associated with the stretching vibrations of Li atoms in pairs.

III. CONCLUSION

In summary, we have designed 12 Li_8H_n electrides whose IAEs charge and topology (e.g., 0D, 1D, 2D, etc.) can be modulated by changing the content and occupation site of hydrogen atoms. A near-linear positive correlation between IAE charge and the EPC is explicitly revealed in them, originating from the coupling of hybridized electrons of IAEs and Li $2p$ with Li-derived low-/medium-frequency phonons, responsible for the T_c evolution. The maximum T_c is predicted in cubic Pm-3m Li_8H_4 with 40.3 K, associated with a unique IAEs dimerization induced by the compressing and stretching vibrations of Li atoms in pairs. This paper provides a significant insight into electride superconductivity, and a powerful guidance for the exploration of new electride superconductors.

ACKNOWLEDGMENTS

The authors acknowledge funding from the National Key Research and Development Program of China (Grant No. 2022YFA1402300), the Natural Science Foundation of China under Grants No. 22372142, No. 12304028, and No. U23A20537, the High-End Foreign Expert Introduction Program (Grant No. G2023003004L), the Central Guiding Local Science and Technology Development Fund Projects (Grant No. 236Z7605G), the Natural Science Foundation of Hebei Province (Grant No. B2021203030), and the Science and Technology Project of Hebei Education Department (Grant No. QN2023246). A.B. acknowledges financial support from the Spanish Ministry of Science and Innovation (Grant No. PID2022-139230NB-I00) and the Department of Education, Universities and Research of the Basque Government and the University of the Basque Country (Grant No. IT1707-22). This work way carried out at the National Supercomputer Center in Tianjin, and the calculations were performed on TianHe-1 (A).

[1] J.-X. Yin, B. Lian, and M. Z. Hasan, Topological kagome magnets and superconductors, Nature (London) **612**, 647 (2022).

[2] J. L. MacManus-Driscoll and S. C. Wimbush, Processing and application of high-temperature superconducting coated conductors, Nat. Rev. Mater. **6**, 587 (2021).

[3] D. Qiu, C. Gong, S. Wang, M. Zhang, C. Yang, X. Wang, and J. Xiong, Recent advances in 2D superconductors, Adv. Mater. **33**, 2006124 (2021).

[4] H. Xie, Y. Yao, X. Feng, D. Duan, H. Song, Z. Zhang, S. Jiang, S. A. T. Redfern, V. Z. Kresin, C. J. Pickard, and T. Cui, Hydrogen pentagraphenelike structure stabilized by hafnium: A high-temperature conventional superconductor, Phys. Rev. Lett. **125**, 217001 (2020).

[5] Z. Zhang, T. Cui, M. J. Hutcheon, A. M. Shipley, H. Song, M. Du, V. Z. Kresin, D. Duan, C. J. Pickard, and Y. Yao, Design principles for high-temperature superconductors with a hydrogen-based alloy backbone at moderate pressure, Phys. Rev. Lett. **128**, 047001 (2022).

[6] H. Wang, J. S. Tse, K. Tanaka, T. Iitaka, and Y. Ma, Superconductive sodalite-like clathrate calcium hydride at high pressures, Proc. Natl. Acad. Sci. USA **109**, 6463 (2012).

[7] H. Liu, I. I. Naumov, R. Hoffmann, N. W. Ashcroft, and R. J. Hemley, Potential high-T_c superconducting lanthanum and yttrium hydrides at high pressure, Proc. Natl. Acad. Sci. USA **114**, 6990 (2017).

[8] F. Peng, Y. Sun, C. J. Pickard, R. J. Needs, Q. Wu, and Y. Ma, Hydrogen clathrate structures in rare earth hydrides at high pressures: Possible route to room-temperature superconductivity, Phys. Rev. Lett. **119**, 107001 (2017).

[9] Y. Sun, J. Lv, Y. Xie, H. Liu, and Y. Ma, Route to a superconducting phase above room temperature in electron-doped hydride compounds under high pressure, Phys. Rev. Lett. **123**, 097001 (2019).

[10] Y. Sun, X. Zhong, H. Liu, and Y. Ma, Clathrate metal superhydrides at high-pressure conditions: Enroute to room-temperature superconductivity, Natl. Sci. Rev. **11**, nwad270 (2024).

[11] H. Hosono and M. Kitano, Advances in materials and applications of inorganic electrides, Chem. Rev. **121**, 3121 (2021).

[12] X. Zhang and G. Yang, Recent advances and applications of inorganic electrides, J. Phys. Chem. Lett. **11**, 3841 (2020).

[13] S. Matsuishi, Y. Toda, M. Miyakawa, K. Hayashi, T. Kamiya, M. Hirano, I. Tanaka, and H. Hosono, High-density electron anions in a nanoporous single crystal: $[Ca_{24}Al_{28}O_{64}]^{4+}(4e^-)$, Science **301**, 626 (2003).

[14] Y. Zhang, Z. Xiao, T. Kamiya, and H. Hosono, Electron confinement in channel spaces for one-dimensional electride, J. Phys. Chem. Lett. **6**, 4966 (2015).

[15] K. Lee, S. W. Kim, Y. Toda, S. Matsuishi, and H. Hosono, Dicalcium nitride as a two-dimensional electride with an anionic electron layer, Nature (London) **494**, 336 (2013).

[16] Y. Tsuji, P. L. V. K. Dasari, S. F. Elatresh, R. Hoffmann, and N. W. Ashcroft, Structural diversity and electron confinement in Li_4N: Potential for 0-D, 2-D, and 3-D electrides, J. Am. Chem. Soc. **138**, 14108 (2016).

[17] M.-s. Miao, R. Hoffmann, J. Botana, I. I. Naumov, and R. J. Hemley, Quasimolecules in compressed lithium, Angew. Chem. Int. Ed. **56**, 972 (2017).

[18] A. Bergara, J. B. Neaton, and N. W. Ashcroft, Pairing, π-bonding, and the role of nonlocality in a dense lithium monolayer, Phys. Rev. B **62**, 8494 (2000).

[19] M.-s. Miao and R. Hoffmann, High-pressure electrides: The chemical nature of interstitial quasiatoms, J. Am. Chem. Soc. **137**, 3631 (2015).

[20] X. Wang, Y. Wang, J. Wang, S. Pan, Q. Lu, H.-T. Wang, D. Xing, and J. Sun, Pressure stabilized lithium-aluminum compounds with both superconducting and superionic behaviors, Phys. Rev. Lett. **129**, 246403 (2022).

[21] X. Zhang, Y. Yao, S. Ding, A. Bergara, F. Li, Y. Liu, X.-F. Zhou, and G. Yang, Superconductivity in Li_8Au electride, Phys. Rev. B **107**, L100501 (2023).

[22] M. Miyakawa, S. W. Kim, M. Hirano, Y. Kohama, H. Kawaji, T. Atake, H. Ikegami, K. Kono, and H. Hosono, Superconductivity in an inorganic electride $12CaO \cdot 7Al_2O_3{:}E^-$, J. Am. Chem. Soc. **129**, 7270 (2007).

[23] Y. Zhang, B. Wang, Z. Xiao, Y. Lu, T. Kamiya, Y. Uwatoko, H. Kageyama, and H. Hosono, Electride and superconductivity behaviors in Mn_5Si_3-type intermetallics, npj Quantum Mater. **2**, 45 (2017).

[24] X. Zeng, S. Zhao, Z. Li, and J. Yang, Electron-phonon interaction in a Ca_2N monolayer: Intrinsic mobility of electrene, Phys. Rev. B **98**, 155443 (2018).

[25] X.-L. Qiu, J.-F. Zhang, H.-C. Yang, Z.-Y. Lu, and K. Liu, Superconductivity in monolayer Ba_2N electride: First-principles study, Phys. Rev. B **105**, 165101 (2022).

[26] Y. Xie, A. R. Oganov, and Y. Ma, Novel high pressure structures and superconductivity of $CaLi_2$, Phys. Rev. Lett. **104**, 177005 (2010).

[27] X. Li, A. Hermann, F. Peng, J. Lv, Y. Wang, H. Wang, and Y. Ma, Stable lithium argon compounds under high pressure, Sci. Rep. **5**, 16675 (2015).

[28] B. Sa, R. Xiong, C. Wen, Y.-L. Li, P. Lin, Q. Lin, M. Anpo, and Z. Sun, Electronic anisotropy and superconductivity in one-dimensional electride Ca_3Si, J. Phys. Chem. C **124**, 7683 (2020).

[29] Y.-X. Liu, C. Wang, S. Han, X. Chen, H.-R. Sun, and X.-B. Liu, Novel superconducting electrides in Ca–S System under high pressures, Chin. Phys. Lett. **38**, 036201 (2021).

[30] Z. Liu, Q. Zhuang, F. Tian, D. Duan, H. Song, Z. Zhang, F. Li, H. Li, D. Li, and T. Cui, Proposed superconducting electride Li_6C by *sp*-Hybridized cage states at moderate pressures, Phys. Rev. Lett. **127**, 157002 (2021).

[31] J. Hou, X. Dong, A. R. Oganov, X.-J. Weng, C.-M. Hao, G. Yang, H.-T. Wang, X.-F. Zhou, and Y. Tian, Helium-bearing superconductor at high pressure, Phys. Rev. B **106**, L220501 (2022).

[32] X. Zhang, F. Li, A. Bergara, and G. Yang, Pressure-induced superconductivity in Li-Te electrides, Phys. Rev. B **104**, 134505 (2021).

[33] Y. Zhao, A. Bergara, X. Zhang, F. Li, Y. Liu, and G. Yang, Interstitial anionic electrons favoring superconductivity in Li-As electrides, Phys. Rev. B **108**, 104505 (2023).

[34] L. Song, X. Jin, J. Li, Y. Liu, L. An, Y. Chen, Q. Jin, T. Cui, and B. Liu, Superconductivity and Wilson transition behaviors of lithium-rich oxides Li_mO ($m = 1$–8) under pressure based on *ab initio Calculations*, Phys. Rev. B **108**, 054102 (2023).

[35] Q. Wang, S. Zhang, H. Li, H. Wang, G. Liu, J. Ma, H. Xu, H. Liu, and Y. Ma, Coexistence of superconductivity and electride states in Ca_2H with an antifluorite-type motif under compression, J. Mater. Chem. A **11**, 21345 (2023).

[36] Z. S. Pereira, G. M. Faccin, and E. Z. da Silva, Predicted superconductivity in the electride Li_5C, J. Phys. Chem. C **125**, 8899 (2021).

[37] Z. Wan, C. Zhang, T. Yang, W. Xu, and R. Zhang, Predicted superconductivity and superionic state in the electride Li_5N under high pressure, New J. Phys. **24**, 113012 (2022).
[38] H.-M. Huang, Q. Zhu, V. A. Blatov, A. R. Oganov, X. Wei, P. Jiang, and Y.-L. Li, Novel topological motifs and superconductivity in Li-Cs System, Nano Lett. **23**, 5012 (2023).
[39] Z. Zhao, S. Zhang, T. Yu, H. Xu, A. Bergara, and G. Yang, Predicted pressure-induced superconducting transition in electride Li_6P, Phys. Rev. Lett. **122**, 097002 (2019).
[40] Z. Liu, D. Duan, Q. Zhuang, and T. Cui, High-temperature superconductivity in electrides dominated by hybridized *p*-orbital-like electride states, Phys. Rev. B **108**, L100507 (2023).
[41] M.-S. Miao and R. Hoffmann, High pressure electrides: A predictive chemical and physical theory, Acc. Chem. Res. **47**, 1311 (2014).
[42] Q. Wang, W. Cui, K. Gao, J. Chen, T. Gu, M. Liu, J. Hao, J. Shi, and Y. Li, Pressure-stabilized superconducting electride Li_5C, Phys. Rev. B **106**, 054519 (2022).
[43] J.-Y. You, B. Gu, G. Su, and Y. P. Feng, Emergent kagome electrides, J. Am. Chem. Soc. **144**, 5527 (2022).
[44] H. Kim, I. Park, J. H. Shim, and D. Y. Kim, Superconductivity of metastable dihydrides at ambient pressure, arXiv:2311.17328.
[45] N. W. Ashcroft, Metallic hydrogen: A high-temperature superconductor? Phys. Rev. Lett. **21**, 1748 (1968).
[46] J. M. McMahon and D. M. Ceperley, High-temperature superconductivity in atomic metallic hydrogen, Phys. Rev. B **84**, 144515 (2011).
[47] Y. Sun and M. Miao, Chemical templates that assemble the metal superhydrides, Chem. **9**, 443 (2023).
[48] S. Yi, C. Wang, H. Jeon, and J.-H. Cho, Stability and bonding nature of clathrate H cages in a near-room-temperature superconductor LaH_{10}, Phys. Rev. Mater. **5**, 024801 (2021).
[49] C. Wang, S. Yi, S. Liu, and J.-H. Cho, Underlying mechanism of charge transfer in Li-doped MgH_{16} at high pressure, Phys. Rev. B **102**, 184509 (2020).
[50] See Supplemental Material at http://link.aps.org/supplemental/10.1103/PhysRevB.109.134505 for detailed computational details, structural information, structure construction diagram, Bader charge, phonon dispersion curves, formation enthalpy, crystal structures and ELF isosurfaces, electronic band structures, superconductivity of Li_8H_n ($n = 4$–7) electrides, and the Fermi surfaces and pressure-dependent superconductivity of *Pm*-3*m* Li_8H_4. It also contains Refs. [51–57].
[51] P. Hohenberg and W. Kohn, Inhomogeneous electron gas, Phys. Rev. **136**, B864 (1964).
[52] W. Kohn and L. J. Sham, Self-consistent equations including exchange and correlation effects, Phys. Rev. **140**, A1133 (1965).
[53] G. Kresse and J. Furthmüller, Efficient iterative schemes for *ab initio* total-energy calculations using a plane-wave basis set, Phys. Rev. B **54**, 11169 (1996).
[54] J. P. Perdew, J. A. Chevary, S. H. Vosko, K. A. Jackson, M. R. Pederson, D. J. Singh, and C. Fiolhais, Atoms, molecules, solids, and surfaces: Applications of the generalized gradient approximation for exchange and correlation, Phys. Rev. B **46**, 6671 (1992).
[55] P. E. Blöchl, Projector augmented-wave method, Phys. Rev. B **50**, 17953 (1994).
[56] A. Togo, F. Oba, and I. Tanaka, First-principles calculations of the ferroelastic transition between rutile-type and $CaCl_2$-type SiO_2 at high pressures, Phys. Rev. B **78**, 134106 (2008).
[57] P. Giannozzi *et al.*, QUANTUM ESPRESSO: A modular and open-source software project for quantum simulations of materials, J. Phys.: Condens. Matter **21**, 395502 (2009).
[58] P. B. Allen and R. C. Dynes, Transition temperature of strong-coupled superconductors reanalyzed, Phys. Rev. B **12**, 905 (1975).
[59] X. Zhong, H. Wang, J. Zhang, H. Liu, S. Zhang, H.-F. Song, G. Yang, L. Zhang, and Y. Ma, Tellurium hydrides at high pressures: High-temperature superconductors, Phys. Rev. Lett. **116**, 057002 (2016).
[60] J. A. Flores-Livas, L. Boeri, A. Sanna, G. Profeta, R. Arita, and M. Eremets, A perspective on conventional high-temperature superconductors at high pressure: Methods and materials, Phys. Rep. **856**, 1 (2020).
[61] H. Hosono, S.-W. Kim, S. Matsuishi, S. Tanaka, A. Miyake, T. Kagayama, and K. Shimizu, Superconductivity in room-temperature stable electride and high-pressure phases of alkali metals, Philos. Trans. R. Soc. A **373**, 20140450 (2015).
[62] F. Belli, T. Novoa, J. Contreras-García, and I. Errea, Strong correlation between electronic bonding network and critical temperature in hydrogen-based superconductors, Nat. Commun. **12**, 5381 (2021).
[63] S. Racioppi, C. V. Storm, M. I. McMahon, and E. Zurek, On the electride nature of Na-hP4, Angew. Chem. Int. Ed. **62**, e202310802 (2023).
[64] X. Dong, A. R. Oganov, H. Cui, X.-F. Zhou, and H.-T. Wang, Electronegativity and chemical hardness of elements under pressure, Proc. Natl. Acad. Sci. USA **119**, e2117416119 (2022).
[65] R. C. Dynes, McMillan's equation and the T_c of superconductors, Solid State Commun. **10**, 615 (1972).
[66] J. Nagamatsu, N. Nakagawa, T. Muranaka, Y. Zenitani, and J. Akimitsu, Superconductivity at 39 K in magnesium diboride, Nature (London) **410**, 63 (2001).
[67] X. Zhang, M. Zhao, and F. Liu, Enhancing superconductivity in bulk β-Bi_2Pd by negative pressure induced by quantum electronic stress, Phys. Rev. B **100**, 104527 (2019).
[68] J. M. An and W. E. Pickett, Superconductivity of MgB_2: Covalent bonds driven metallic, Phys. Rev. Lett. **86**, 4366 (2001).
[69] H. J. Choi, D. Roundy, H. Sun, M. L. Cohen, and S. G. Louie, The origin of the anomalous superconducting properties of MgB_2, Nature (London) **418**, 758 (2002).
[70] J. Bekaert, M. Petrov, A. Aperis, P. M. Oppeneer, and M. V. Milošević, Hydrogen-induced high-temperature superconductivity in two-dimensional materials: The example of hydrogenated monolayer MgB_2, Phys. Rev. Lett. **123**, 077001 (2019).
[71] F. Zheng, Y. Sun, R. Wang, Y. Fang, F. Zhang, S. Wu, C.-Z. Wang, V. Antropov, and K.-M. Ho, Superconductivity in the Li-B-C system at 100 GPa, Phys. Rev. B **107**, 014508 (2023).
[72] X. Liu, X. Huang, P. Song, C. Wang, L. Zhang, P. Lv, L. Liu, W. Zhang, J.-H. Cho, and Y. Jia, Strong electron-phonon coupling superconductivity in compressed α-MoB_2 induced by double Van Hove singularities, Phys. Rev. B **106**, 064507 (2022).
[73] F. S. Khan and P. B. Allen, Deformation potentials and electron-phonon scattering: Two new theorems, Phys. Rev. B **29**, 3341 (1984).